

RESONANCE, MULTIPLE DIFFUSION AND CRITICAL TUNNELING FOR GAUSSIAN LASERS

Silvânia A. Carvalho and Stefano De Leo*

Department of Applied Mathematics, State University of Campinas, Brazil

• EUROPEAN PHYSICAL JOURNAL D **67**, 168-11 (2013) •

Abstract

We present a detailed study of the gaussian laser propagation through a dielectric system composed by two right angle prisms. We investigate the transition between the spatial coherence limit, which exhibits wave-like properties and for which the resonance phenomenon can be seen, and the decoherence limit, which exhibits particle-like properties and for which the multiple diffusion occurs. We also analyze the tunneling at critical angles. In our numerical analysis, we shall use BK7 and Fused Silica prisms and a gaussian *He-Ne* laser with a wavelength of 632.8 nm and beam waists of 2 mm and 200 μm .

I. INTRODUCTION

Total internal reflection in single right angle prism experiments has been the subject of a deep study in the last decades [1–6]. This phenomenon continues to be a topic of great scientific interest because an additional phase is present in the reflected beam when totally reflected. This phase is responsible for the (Goos-Hänchen) shift [7] in the reflected beam. This shift is the optical counterpart of the well known delay time of quantum mechanics [8–10].

The double right angle prism apparatus, see Fig. 1, represents a fascinating arrangement to display both wave and particle-like propagation of light [11, 12] and to frustrate total internal reflection [13–19]. In this paper, we shall use the wave packet formalism (gaussian beams) to describe the light propagation. The wave behavior is obviously recovered in the limit in which the beam waist is very large with respect to the air interspace between the two right angle prisms. The formalism used in this paper is the same presented in [12], but, with respect to the single dielectric block, the double prisms apparatus present the additional phenomenon of frustrated total internal reflection, amplified for incidence at *critical* angles. The use of wave packets introduces a *new* parameter (the beam waist) in the numerical analysis. We investigate for BK7 and Fused Silica prisms and gaussian *He-Ne* lasers how resonance, multiple diffusion and critical tunneling are related to this parameter. Of particular interest, it will be the study of the limit case between wave and particle-like light propagation, i.e. the case of *partial coherence*. The analytical and numerical prediction shed new light on the transition between resonance and multiple diffusion and can be tested experimental.

II. PARAXIAL APPROXIMATION AND GAUSSIAN LASER BEAM AMPLITUDE

Gaussian beams are the simplest and often the most common type of beam provided by a laser source. Their behavior is described by a few parameters such as the spot size, the radius of curvature, and the Gouy phase [20, 21]. In this section, we introduce the wave number convolution of plane waves which, in the limit of paraxial approximation, allows to obtain the standard analytic expression for a gaussian beam moving in free space. This convolution function, modulated by the reflection and transmission coefficients obtained by imposing continuity at each interface, will be then used to calculate the intensity of the outgoing beams which propagate through the two right angle dielectric prisms separated by an air gap.

*deleo@ime.unicamp.br

Our analysis is done for time-harmonic waves, $\omega (= 2\pi c/\lambda)$. This implies a stationary system. So, we can forego writing the time dependence $\exp[-i\omega t]$. For our theoretical analysis, we start with plane waves which correspond to momentum eigenvalues, $\exp[i\mathbf{k} \cdot \mathbf{r}]$. They determine a fixed propagation direction \mathbf{k} . The electric field can be then expressed by $\exp[i\mathbf{k} \cdot \mathbf{r} - \omega t] \hat{\mathbf{s}}$. The condition $\nabla \cdot \mathbf{E} = 0$, imposed by one of the Maxwell equations implies $\hat{\mathbf{s}} \cdot \mathbf{k} = 0$, and consequently the electric field vector lies in the plane perpendicular to the direction of propagation \mathbf{k} . Electromagnetic waves can oscillate with more than one orientation. By convention, the polarization is described by specifying the orientation of the electric field. For different plane wave directions, the polarization vector necessarily changes.

A general solution can then be obtained by convoluting plane waves with a suitable integral

$$\mathbf{E}(\mathbf{r}, t) = E_0 \int d\mathbf{k} G(k_x, k_y) \delta\left(k_z - \sqrt{k^2 - k_x^2 - k_y^2}\right) \exp[i(\mathbf{k} \cdot \mathbf{r} - \omega t)] \hat{\mathbf{s}}, \quad (1)$$

where $k = |\mathbf{k}|$. The Dirac delta function and the condition $k = \omega/c$ guarantee that each electric field component satisfies the wave equation

$$\left(c^2 \nabla^2 - \partial_t^2\right) \mathbf{E}(\mathbf{r}, t) = 0. \quad (2)$$

For a sharp wave number distribution, $k_{x,y} \ll k$, the beam is sufficiently collimated along the z axis. Consequently, we can use the following approximation

$$k_z \approx k - \frac{k_x^2 + k_y^2}{2k}.$$

Taking as plane of incidence the y - z plane, we may assume to a good approximation that the electric vector is given by $\mathbf{E} = \{E_s, E_p, 0\}$, where E_s is the component of the electric field perpendicular to the plane of incidence (s -polarization) and E_p is the component parallel to this plane (p -polarization). To simplify our presentation, we shall suppose that the laser beam passes through a polarizer which selects the s -polarization,

$$\begin{aligned} \mathbf{E}(\mathbf{r}, t) &\approx E_0 e^{i(kz - \omega t)} \int dk_x dk_y G(k_x, k_y) \exp\left[i\left(k_x x + k_y y - \frac{k_x^2 + k_y^2}{2k} z\right)\right] \hat{\mathbf{x}} \\ &= E_0 e^{i(kz - \omega t)} A(x, y, z) \hat{\mathbf{x}}. \end{aligned} \quad (3)$$

The field $A(x, y, z)$ satisfies the paraxial wave equation [22]

$$(\partial_{xx} + \partial_{yy} + 2ik\partial_z) A(x, y, z) = 0. \quad (4)$$

Solving this equation yields an infinite set of functions of which the gaussian beam is the lowest-order mode,

$$G(k_x, k_y) = \frac{w_0^2}{4\pi} \exp\left[-\frac{(k_x^2 + k_y^2) w_0^2}{4}\right].$$

The use of the paraxial gaussian approximation is justified for beam waists, w_0 , satisfying $k w_0 \geq 5$. From

$$A(x, y, z) = \frac{w_0^2}{4\pi} \int dk_x dk_y \exp\left[-\frac{(k_x^2 + k_y^2) w_0^2}{4}\right] \exp\left[i\left(k_x x + k_y y - \frac{k_x^2 + k_y^2}{2k} z\right)\right], \quad (5)$$

after performing two generalized gaussian integrations, we obtain the well-known closed formula which describe the free propagation of a gaussian laser beam

$$E(x, y, z) = E_0 e^{i(kz - \omega t)} \frac{w_0}{w(z)} \exp\left[-\frac{x^2 + y^2}{w^2(z)} + i\frac{(x^2 + y^2)k}{2R(z)} - i\phi(z)\right], \quad (6)$$

where

$$w(z) = w_0 \sqrt{1 + \left(\frac{2z}{k w_0^2} \right)^2} = w_0 \sqrt{1 + \left(\frac{z}{z_R} \right)^2}$$

represents the radius at which the field amplitude drop to $1/e$ of its axial value, z_R is the Rayleigh range, $R(z) = z(1 + z_R^2/z^2)$ is the radius of curvature of the wavefront of the gaussian beam, and $\phi = \arctan[z/z_R]$ is the longitudinal phase delay also know as Gouy phase. The corresponding intensity distribution is

$$I(x, y, z) = I_0 \left[\frac{w_0}{w(z)} \right]^2 \exp \left[-2 \frac{x^2 + y^2}{w^2(z)} \right], \quad (7)$$

and the total power of the beam is $P_0 = \pi w_0^2 I_0 / 2$.

III. GEOMETRY OF THE DIELECTRIC SYSTEM

In Fig. 1, we show the y - z overview of the double prism dielectric layout. The double prism structure is created by air zones separating two right angle prisms made of the same dielectric material of refractive index n . The incident gaussian beam propagates along the z -axis,

$$[\nabla(\mathbf{k} \cdot \mathbf{r})]_{(k_x=0, k_y=0)} = (0, 0, k), \quad (8)$$

and forms an angle θ with z_{up} , normal to the dielectric block,

$$x_{up} = x \quad \text{and} \quad \begin{pmatrix} y_{up} \\ z_{up} \end{pmatrix} = \begin{pmatrix} \cos \theta & \sin \theta \\ -\sin \theta & \cos \theta \end{pmatrix} \begin{pmatrix} y \\ z \end{pmatrix} = R(\theta) \begin{pmatrix} y \\ z \end{pmatrix}. \quad (9)$$

Observing that $z_{up} = z_{down}$ and that the two right angle prisms are separated by a parallel air gap, the down side outgoing beam has the same spatial phase of the incoming beam,

$$\mathbf{k}_{down} \cdot \mathbf{r}_{down} = \mathbf{k}_{up} \cdot \mathbf{r}_{up} = \mathbf{k} \cdot \mathbf{r}.$$

For the right side outgoing beam the situation is a little bit more complicated. In this case, it is useful to introduce the following rotations

$$x_{right} = x_* = x_{up} \quad \text{and} \quad \begin{pmatrix} y_{right} \\ z_{right} \end{pmatrix} = R\left(-\frac{3\pi}{4}\right) \begin{pmatrix} y_* \\ z_* \end{pmatrix} = R\left(-\frac{\pi}{2}\right) \begin{pmatrix} y_{up} \\ z_{up} \end{pmatrix}. \quad (10)$$

Due to the fact that the first air/dielectric discontinuity is along z_{up} axis, we have

$$q_{x_{up}} = k_{x_{up}} = k_x \quad \text{and} \quad q_{y_{up}} = k_{y_{up}} = k_y \cos \theta + \sqrt{k^2 - k_x^2 - k_y^2} \sin \theta.$$

Consequently, the spatial phase of the transmitted beam which propagates in the first dielectric block is given by

$$\mathbf{q}_{up} \cdot \mathbf{r}_{up} = k_x x + k_{y_{up}} y_{up} + \sqrt{n^2 k^2 - k_x^2 - k_{y_{up}}^2} z_{up}. \quad (11)$$

It is interesting to observe that for $k_{x,y} \rightarrow 0$, we find

$$nk(\sin \psi, \cos \psi) := (q_{y_{up}}, q_{z_{up}}) \rightarrow k(\sin \theta, \sqrt{n^2 - \sin^2 \theta}) \Rightarrow \sin \theta = n \sin \psi.$$

Thus, the condition that the wave number component perpendicular to the normal of the air/dielectric discontinuity does not change, $q_{y_{up}} = k_{y_{up}}$, allows to recover, in the limit of plane wave, the well known refraction Snell law. The spatial phase of the beam which propagates from the transversal air/dielectric discontinuity towards the diagonal dielectric/air discontinuity in the first prism can be rewritten in terms of the y_* - z_* axes as follows

$$\mathbf{q}_* \cdot \mathbf{r}_* = \mathbf{q}_{up} \cdot \mathbf{r}_{up},$$

where

$$q_{x_*} = q_{x_{up}} = k_x \quad \text{and} \quad \begin{pmatrix} q_{y_*} \\ q_{z_*} \end{pmatrix} = R\left(\frac{\pi}{4}\right) \begin{pmatrix} q_{y_{up}} \\ q_{z_{up}} \end{pmatrix}.$$

The spatial phase of the reflected beam at the air gap is then obtained by replacing q_{z_*} with $-q_{z_*}$. Observing that

$$q_{x_{right}} = q_{x_*} = k_x \quad \text{and} \quad \begin{pmatrix} q_{y_{right}} \\ q_{z_{right}} \end{pmatrix} = R\left(-\frac{3\pi}{4}\right) \begin{pmatrix} q_{y_*} \\ -q_{z_*} \end{pmatrix} = \begin{pmatrix} -q_{y_{up}} \\ q_{z_{up}} \end{pmatrix} = \begin{pmatrix} -k_{y_{up}} \\ q_{z_{up}} \end{pmatrix},$$

the reflected beam, propagating from the diagonal dielectric/air interface to the right side dielectric/air discontinuity, will have the following spatial phase

$$k_x x - k_{y_{up}} y_{right} + \sqrt{n^2 k^2 - k_x^2 - k_{y_{up}}^2} z_{right}. \quad (12)$$

Due to the fact that the right dielectric/discontinuity is along the z_{right} axis, we have

$$k_{x_{right}} = q_{x_{right}} = k_x \quad \text{and} \quad k_{y_{right}} = q_{y_{right}} = -k_{y_{up}}.$$

Finally, the spatial phase of the right side outgoing beam is

$$\begin{aligned} \mathbf{k}_{right} \cdot \mathbf{r}_{right} &= k_x x + k_{y_{up}} z_{up} + \sqrt{k^2 - k_x^2 - k_{y_{up}}^2} y_{up} \\ &= k_x x + [k_z \cos(2\theta) - k_y \sin(2\theta)] y + [k_z \sin(2\theta) + k_y \cos(2\theta)] z, \end{aligned} \quad (13)$$

where $k_z = \sqrt{k^2 - k_x^2 - k_y^2}$. The wave number vector of the right side outgoing beam is then given by

$$[\nabla \varphi_{right}]_{(k_x=0, k_y=0)} = [0, k \cos(2\theta), k \sin(2\theta)]. \quad (14)$$

Whereas the down side outgoing beam and the incoming beam are always parallel, the right side outgoing beam and the incoming beam are parallel only for the incident angle $\theta = \pi/4$. Once obtained the spatial phases, to calculate the intensities of the outgoing beams, we need to find how the wave number distribution is modified by reflection and transmission at each interface. For the right side outgoing amplitude, the convolution function is obtained by multiplying the incoming gaussian distribution by the transmission and reflection coefficients obtained by imposing continuity at the first transversal air/dielectric discontinuity, T_{up} , at the air gap, R_* , and at the (right) dielectric/air interface, T_{right} ,

$$A_{right}(x, y, z) = \frac{w_0^2}{4\pi} \int dk_x dk_y T_{up} R_* T_{right} \exp \left[-\frac{(k_x^2 + k_y^2) w_0^2}{4} + i \mathbf{k}_{right} \cdot \mathbf{r}_{right} \right]. \quad (15)$$

In a similar way, the down side outgoing amplitude is given by

$$A_{down}(x, y, z) = \frac{w_0^2}{4\pi} \int dk_x dk_y T_{up} T_* T_{down} \exp \left[-\frac{(k_x^2 + k_y^2) w_0^2}{4} + i \mathbf{k} \cdot \mathbf{r} \right] \quad (16)$$

where T_* is the transmission amplitude for the beam propagating through the air gap between the two right angle prisms and T_{down} is the coefficient for the transmission through the (down) dielectric/air interface.

IV. REFLECTION AND TRANSMISSION COEFFICIENTS

Maxwells equations describe optical phenomena and under certain conditions present a surprising aspect, they mimic the quantum mechanical Schrödinger equation [23, 24]. The counterpart of the energy potential in quantum mechanics is represented by the stratified dielectric medium with which

the laser interacts [10–12,25]. The reflection and transmission amplitudes both in optics and quantum mechanics can be built by imposing continuity at dielectric or potential discontinuities.

The incoming plane wave is

$$\exp[i \mathbf{k} \cdot \mathbf{r}] = \exp[i \mathbf{k}_{up} \cdot \mathbf{r}_{up}] .$$

For a dielectric block stratified along the z_{up} direction, the separation of variables implies that the wave number in the $x_{up}(=x)$ and y_{up} directions remain unaltered, $q_{x_{up}} = k_{x_{up}} = k_x$ and $q_{y_{up}} = k_{y_{up}}$. Only the z_{up} wave number changes. The continuity equations at the air/dielectric discontinuity

$$\left[\exp[i k_{z_{up}} z_{up}] + R_{up} \exp[-i k_{z_{up}} z_{up}] \right]_{z_{up}=d_{up}} = \left[T_{up} \exp[i q_{z_{up}} z_{up}] \right]_{z_{up}=d_{up}}$$

and

$$\left[\partial_{z_{up}} \left(\exp[i k_{z_{up}} z_{up}] + R_{up} \exp[-i k_{z_{up}} z_{up}] \right) \right]_{z_{up}=d_{up}} = \left[\partial_{z_{up}} T_{up} \exp[i q_{z_{up}} z_{up}] \right]_{z_{up}=d_{up}}$$

yield

$$T_{up} = \frac{2 k_{z_{up}}}{k_{z_{up}} + q_{z_{up}}} \exp[i (k_{z_{up}} - q_{z_{up}}) d_{up}] . \quad (17)$$

The transmission coefficients through the right and down dielectric interfaces can be immediately obtained from the previous one by the following substitutions

$$k_{z_{up}} \rightarrow q_{z_{right,down}} = q_{z_{up}} , \quad q_{z_{up}} \rightarrow k_{z_{right,down}} = k_{z_{up}} \quad \text{and} \quad d_{up} \rightarrow d_{right,down} .$$

Consequently,

$$T_{right,down} = \frac{2 q_{z_{up}}}{q_{z_{up}} + k_{z_{up}}} \exp[i (q_{z_{up}} - k_{z_{up}}) d_{right,down}] . \quad (18)$$

The air gap between the right angle prisms simulates a quantum mechanical barrier of width h_* . The general z_* solution in the air gap

$$A_* \exp[i k_{z_*} z_*] + B_* \exp[-i k_{z_*} z_*]$$

can be oscillatory or evanescent depending if

$$k_{z_*}^2 = k^2 - k_x^2 - k_{y_*}^2$$

is positive or negative. Expanding $k_{z_*}^2$ at first order in k_y , we find

$$k_{z_*}^2 = k^2 \left(1 - \frac{n^2}{2} - \sin \theta \sqrt{n^2 - \sin^2 \theta} \right) - k k_y \cos \theta \frac{n^2 - 2 \sin^2 \theta}{\sqrt{n^2 - \sin^2 \theta}} + \text{O} \left[k_x^2, k_y^2 \right] . \quad (19)$$

Consequently, we find evanescent waves for $k_y > \sigma(n, \theta) k$ and oscillatory waves for $k_y < \sigma(n, \theta) k$, where

$$\sigma(n, \theta) = \frac{2 - n^2 - 2 \sin \theta \sqrt{n^2 - \sin^2 \theta}}{2 \cos \theta (n^2 - 2 \sin^2 \theta)} \sqrt{n^2 - \sin^2 \theta} . \quad (20)$$

At critical angles,

$$\sin \theta_c \sqrt{n^2 - \sin^2 \theta_c} = 1 - \frac{n^2}{2} , \quad (21)$$

$\sigma(n, \theta) = 0$ and our wave packet will have the same amount of evanescent ($k_y > 0$) and oscillatory ($k_y < 0$) waves. By imposing continuity of the electric field and its derivative at the air gap discontinuities, $z_* = d_*$ and $z_* = d_* + h_*$, we find

$$R_* = -i \frac{q_{z_*}^2 - k_{z_*}^2}{2 q_{z_*} k_{z_*}} \frac{\sin(k_{z_*} h_*)}{\mathcal{D}_*} \exp[2 i q_{z_*} d_*] \quad \text{and} \quad T_* = \frac{\exp[-i q_{z_*} h_*]}{\mathcal{D}_*} , \quad (22)$$

where

$$\mathcal{D}_* = \cos(k_{z_*} h_*) - i \frac{q_{z_*}^2 + k_{z_*}^2}{2 q_{z_*} k_{z_*}} \sin(k_{z_*} h_*) .$$

V. RESONANCE AND MULTIPLE DIFFUSION

In order to understand the transition between the coherence (wave-like behavior) and decoherence (particle-like behavior) limit, let us observe that, for *oscillatory waves* propagating across the air gap, the reflection and transmission coefficients given in Eq. (22) can be decomposed in terms of multiple reflection and transmission terms [12] (see refs. [26, 27] for the quantum mechanical analog)

$$R_* = R_*^{(1)} + T_*^{(1)} R_*^{(2)} \sum_{m=0}^{\infty} \left(\tilde{R}_*^{(1)} R_*^{(2)} \right)^m \tilde{T}_*^{(1)} \quad \text{and} \quad T_* = T_*^{(1)} \sum_{m=0}^{\infty} \left(\tilde{R}_*^{(1)} R_*^{(2)} \right)^m T_*^{(2)}, \quad (23)$$

where

$$R_*^{(1)} = \frac{q_{z_*} - k_{z_*}}{q_{z_*} + k_{z_*}} \exp[2i q_{z_*} d_*] \quad \text{and} \quad T_*^{(1)} = \frac{2q_{z_*}}{q_{z_*} + k_{z_*}} \exp[i(q_{z_*} - k_{z_*}) d_*]$$

are the reflection and transmission coefficients for the wave which moving through the first dielectric block encounters the dielectric/air interface at $z_* = d_*$,

$$R_*^{(2)} = \frac{k_{z_*} - q_{z_*}}{k_{z_*} + q_{z_*}} \exp[2i k_{z_*} (d_* + h_*)] \quad \text{and} \quad T_*^{(2)} = \frac{2k_{z_*}}{k_{z_*} + q_{z_*}} \exp[i(k_{z_*} - q_{z_*}) (d_* + h_*)]$$

are the reflection and transmission coefficients for the wave which moving across the air interspace reaches the second dielectric block at $z_* = d_* + h_*$, and

$$\tilde{R}_*^{(1)} = \frac{k_{z_*} - q_{z_*}}{k_{z_*} + q_{z_*}} \exp[-2i k_{z_*} d_*] \quad \text{and} \quad \tilde{T}_*^{(1)} = \frac{2k_{z_*}}{k_{z_*} + q_{z_*}} \exp[i(q_{z_*} - k_{z_*}) d_*],$$

are the reflection and transmission coefficients for the wave which, reaching the second dielectric block, propagating backwards to the first dielectric block interface at $z_* = d_*$.

The phase difference between two successive contributions to reflection or transmission is given by the phase of the loop factor $\tilde{R}_*^{(1)} R_*^{(2)}$. By using the stationary phase method, we can estimate the shift between two successive reflected or transmitted beams, i.e.

$$2 \left[\frac{\partial k_{z_*}}{\partial k_y} \right]_{(0,0)} h_* = \frac{(2 \sin^2 \theta - n^2) \cos \theta \sqrt{2}}{\sqrt{n^2 - \sin^2 \theta} \sqrt{2 - n^2 - 2 \sin \theta \sqrt{n^2 - \sin^2 \theta}}} h_*.$$

For $h_* \ll w_0$ (plane wave limit), the contributions in Eq.(23) overlap and the beam manifests wave-like properties and coherent interference. In such a limit, the relative power for the down/right-side outgoing beams is given by

$$\begin{aligned} \frac{P_{down}^{[wav]}}{P_0} &= |T_{up} T_* T_{down}|_{(0,0)}^2 = \frac{16 \cos^2 \theta (n^2 - \sin^2 \theta)}{(\cos \theta + \sqrt{n^2 - \sin^2 \theta})^4 \left\{ 1 + \frac{(n^2 - 1)^2 \sin^2 [f(n, \theta) k h_*]}{4 [n^2 - 1 + f^2(n, \theta)] f^2(n, \theta)} \right\}}, \\ \frac{P_{right}^{[wav]}}{P_0} &= |T_{up} R_* T_{right}|_{(0,0)}^2 = |T_{up} R_* T_{down}|_{(0,0)}^2 = \frac{16 \cos^2 \theta (n^2 - \sin^2 \theta)}{(\cos \theta + \sqrt{n^2 - \sin^2 \theta})^4} - \frac{P_{down}^{[wav]}}{P_0}, \end{aligned} \quad (24)$$

where

$$f(n, \theta) = \sqrt{1 - \frac{n^2}{2} - \sin \theta \sqrt{n^2 - \sin^2 \theta}}.$$

For $\theta < \theta_c$, $f(n, \theta)$ is a real positive number. Analysis of the behavior of the relative powers shows that resonances are found for

$$f(n, \theta_m) = m \frac{\pi}{k h_*} = m \frac{\lambda}{2 h_*}, \quad (25)$$

where m is a positive integer number. In Table 1, we give the first down-side outgoing beam resonance angles for BK7 and Fused Silica right angle prisms when the incident wavelength is $\lambda = 632.8$ nm. For small angles, a good approximation for $f(n, \theta_m)$ is given by

$$f^2(n, \theta_m) \approx 1 - \frac{n^2}{2} - n \theta_m .$$

From Eq.(25), we obtain

$$\theta_m \approx \frac{1}{n} \left[1 - \left(m \frac{\lambda}{2 h_*} \right)^2 \right] - \frac{n}{2} \quad \Rightarrow \quad \delta \theta_m = \theta_{m+1} - \theta_m \approx - \frac{1 + 2m}{4n} \left(\frac{\lambda}{h_*} \right)^2 . \quad (26)$$

This clearly shows that, for a fixed interval of incidence angles, the numbers of the resonances increases for increasing values of h_* and that, for a given air gap, the resonance width increases for decreasing incidence angles. This behavior is also valid for the general case as it is clearly shown in the power contour plots drawn in Fig. 2.

Let us now analyze the case in which the contributions in Eq.(23) do *not* overlap, this happens for h_* greater than w_0 . In this case, incoherence reigns and the beams manifest a particle-like behavior. In such a limit, we have to consider the sum of the modulus squared of all contributions to reflection,

$$|R_*|_{[par]}^2 = |R_*^{(1)}|^2 + \frac{|T_*^{(1)} R_*^{(2)} \tilde{T}_*^{(1)}|^2}{1 - |\tilde{R}_*^{(1)} R_*^{(2)}|^2} = \frac{(q_{z_*} - k_{z_*})^2}{q_{z_*}^2 + k_{z_*}^2} , \quad (27)$$

and to transmission,

$$|T_*|_{[par]}^2 = \frac{|T_*^{(1)} T_*^{(2)}|^2}{1 - |\tilde{R}_*^{(1)} R_*^{(2)}|^2} = \frac{2 q_{z_*} k_{z_*}}{q_{z_*}^2 + k_{z_*}^2} . \quad (28)$$

The relative power for the down/right-side outgoing beams is now given by

$$\begin{aligned} \frac{P_{down}^{[par]}}{P_0} &= \left[|T_{up}|^2 \frac{2 q_{z_*} k_{z_*}}{q_{z_*}^2 + k_{z_*}^2} |T_{down}|^2 \right]_{(0,0)} \\ &= \frac{16 \cos^2 \theta (n^2 - \sin^2 \theta)}{(\cos \theta + \sqrt{n^2 - \sin^2 \theta})^4} \frac{(\sqrt{n^2 - \sin^2 \theta} - \sin \theta) \sqrt{2} f(n, \theta)}{1 - 2 \sin \theta \sqrt{n^2 - \sin^2 \theta}} , \\ \frac{P_{right}^{[par]}}{P_0} &= \left[|T_{up}|^2 \frac{(q_{z_*} - k_{z_*})^2}{q_{z_*}^2 + k_{z_*}^2} |T_{right}|^2 \right]_{(0,0)} = \frac{16 \cos^2 \theta (n^2 - \sin^2 \theta)}{(\cos \theta + \sqrt{n^2 - \sin^2 \theta})^4} - \frac{P_{down}^{[par]}}{P_0} . \end{aligned} \quad (29)$$

In the particle limit, the power of the outgoing beams, as it is expected, do *not* depend on the air gap distance between the right angle prisms. This is due to the fact that for h_* greater than w_0 the air gap (quantum barrier in quantum mechanics) has to be treated as two separated air interfaces (the two step limit of quantum mechanics). In Table 2, we give the power of the down-side outgoing beam for different incidence angles.

We conclude this section observing that, for oscillatory waves, the amplitudes which appear in Eqs.(22) when summed lead to the amplitudes of Eq.(23). In the wave packet formalism, the gaussian beams, depending on the ratio between the air gap distance and their beam waists, will automatically take into account whether the single contributions overlap or do no overlap. The theoretical result obtained in this section will be tested in section VI by numerical calculations from which we can also see the transition between the wave and particle-like behavior.

VI. CRITICAL TUNNELING

For $\theta > \theta_c$,

$$\theta_c = \begin{cases} + \arcsin \sqrt{(n^2/2) - \sqrt{n^2 - 1}} & \text{for } n < \sqrt{2}, \\ - \arcsin \sqrt{(n^2/2) - \sqrt{n^2 - 1}} & \text{for } n > \sqrt{2}, \end{cases} \quad (30)$$

due to the fact that in Eqs.(24) we have

$$\frac{\sin[f(n, \theta) k h_*]}{f(n, \theta)} = \frac{\sin[i|f(n, \theta)| k h_*]}{i|f(n, \theta)|} = \frac{\sinh[|f(n, \theta)| k h_*]}{|f(n, \theta)|},$$

an exponential decay characterizes the transmission of light across the air gap. For a fixed air gap (see Table 3), we experience, by changing the incidence angle θ , the phenomenon of frustrated total internal reflection and consequently tunneling of light. The transmission is maximized for incidence angles which approach to critical angles, $f(n, \theta_c) \rightarrow 0$. For such angles, we find

$$\begin{aligned} \frac{P_{down}^{[c]}}{P_0} &= \frac{16 \cos^2 \theta (n^2 - \sin^2 \theta)}{(\cos \theta + \sqrt{n^2 - \sin^2 \theta})^4 \left[1 + \frac{(n^2 - 1)(k h_*)^2}{4} \right]}, \\ \frac{P_{right}^{[c]}}{P_0} &= \frac{(n^2 - 1)(k h_*)^2}{4} \frac{P_{down}^{[c]}}{P_0}. \end{aligned} \quad (31)$$

In Fig. 3, we plot the relative power for the down/right-side outgoing *He-Ne* beams. The evanescent waves propagate across the air gap and reaching the second dielectric block allow the phenomenon of frustrated total internal reflection. The contour plots show that this effect is amplified for decreasing values of the air gap distance between the right angle prisms and/or of the incidence angle. Consequently, experiments with incidence angles near to critical angles are more favorable to show the tunneling of light.

VII. NUMERICAL ANALYSIS

Up to now, we have presented analytical expressions for the relative power of the down/right-side outgoing beams. In the case of diffusion, we have discussed two limits. The plane wave limit, see Eq.(24), which we expect to be a good approximation for wave packets with beam waists $w_0 \gg h_*$, and the particle limit, see Eq.(29), which we expect to be valid for air gaps, h_* greater than the beam waists, w_0 . Obviously there is an intermediate situation which should reconcile these clear different limits. The transition between the wave and particle-like behavior is the subject matter of our numerical investigation. The numerical analysis will be also useful to test the theoretical prediction given in the previous sections.

We focus our attention on the power of the down-side outgoing beam. It is clear that a very similar analysis can be easily repeated for the right-side outgoing beam. To calculate the power of the down-side outgoing beam, we have to numerically solve the following integral

$$P_{down} = I_0 \int dx dy |A_{down}(x, y, z)|^2. \quad (32)$$

By using the formula (16), given in section III, for $A_{down}(x, y, z)$, the numerical calculation of the down-side outgoing beam power seems to require to solve six integrals,

$$\begin{aligned} P_{down} &= I_0 \left(\frac{w_0^2}{4\pi} \right)^2 \int dx dy dk_x dk_y d\tilde{k}_x d\tilde{k}_y \times \\ &\quad [T_{up} T_* T_{down}]_{(k_x, k_y)} \exp \left[-\frac{(k_x^2 + k_y^2) w_0^2}{4} + i \mathbf{k} \cdot \mathbf{r} \right] \times \\ &\quad \overline{[T_{up} T_* T_{down}]_{(\tilde{k}_x, \tilde{k}_y)}} \exp \left[-\frac{(\tilde{k}_x^2 + \tilde{k}_y^2) w_0^2}{4} - i \tilde{\mathbf{k}} \cdot \mathbf{r} \right]. \end{aligned}$$

Nevertheless, the spatial integrations can be immediately done leading to two Dirac delta functions,

$$(2\pi)^2 \delta(k_x - \tilde{k}_x) \delta(k_y - \tilde{k}_y) .$$

Making use of these delta functions, we find

$$P_{down} = I_0 \frac{w_0^4}{4} \int dk_x dk_y |T_{up} T_* T_{down}|_{(k_x, k_y)}^2 \exp \left[-\frac{(k_x^2 + k_y^2) w_0^2}{2} \right] . \quad (33)$$

The relative power is then given by

$$\frac{P_{down}}{P_0} = \frac{w_0^2}{2\pi} \int dk_x dk_y |T_{up} T_* T_{down}|_{(k_x, k_y)}^2 \exp \left[-\frac{(k_x^2 + k_y^2) w_0^2}{2} \right] . \quad (34)$$

Observing that the motion is on the y - z plane, the transmission coefficients are characterized by a linear dependence on k_y and a quadratic dependence on k_x . Thus, for a narrow gaussian distribution (typical distribution for gaussian lasers) a good approximation for the relative power is given by

$$\frac{P_{down}}{P_0} \approx \frac{w_0}{\sqrt{2\pi}} \int dk_y |T_{up} T_* T_{down}|_{(0, k_y)}^2 \exp \left[-\frac{k_y^2 w_0^2}{2} \right] . \quad (35)$$

In our numerical calculation, we use *He-Ne* gaussian laser with $\lambda = 632.8$ nm and beam waists of $200 \mu\text{m}$ and 2 mm. This implies narrow distributions, $kw_0 \gg 1$. Consequently, the numerical analysis done by using Eq.(35) shows excellent agreement with the one done with Eq.(34). In Fig. 4 (BK7 right angle prisms) and Fig. 5 (Fused Silica right angle prisms), we plot the relative power for the down-side outgoing beam for different values of the air gap interspace. For $h_* \ll w_0$, we recover the plane wave limit with the resonance phenomenon predicted by Eq.(24). For increasing values of the air gap interspace, the amplitude of the oscillations reduces reaching the particle limit where multiple diffusion occurs and where as it is predicted by Eq.(29), we lost the dependence on the air gap distance between the dielectric blocks. In Figs. 4 and 5, it is clear how the transition happens and how it is possible to reconcile the wave and particle-like behavior. The numerical analysis also shows that the number of oscillations in a given interval is independent of the beam waist. The dependence on the beam waist is seen in how the oscillations are damped.

In the case of *partial coherence*, $h_* \lesssim w_0$, we can give a formula to estimate this damping. As mentioned before, for $h_* \ll w_0$, we reproduce the plane wave limit and, consequently, the relative power for the down-side outgoing beams oscillates between a maximum and minimum value,

$$\begin{aligned} \Delta[h_* \ll w_0] &= \frac{P_{down, \max}^{[wav]}}{P_0} - \frac{P_{down, \min}^{[wav]}}{P_0} = |T_{up} T_{down}|_{(0,0)}^2 \left\{ 1 - \left[\frac{2q_{z_*} k_{z_*}}{q_{z_*}^2 + k_{z_*}^2} \right]_{(0,0)}^2 \right\} \\ &= |T_{up} T_{down}|_{(0,0)}^2 \left[\frac{q_{z_*}^2 - k_{z_*}^2}{q_{z_*}^2 + k_{z_*}^2} \right]_{(0,0)}^2 . \end{aligned} \quad (36)$$

By using

$$k_{z_*} \approx k_{z_*}^{(0,0)} + \left[\frac{\partial k_{z_*}}{\partial k_y} \right]_{(0,0)} k_y ,$$

we can develop the sine term as follows,

$$\begin{aligned} \sin(k_{z_*} h_*) &\approx \sin(k_{z_*}^{(0,0)} h_*) \cos \left(\left[\frac{\partial k_{z_*}}{\partial k_y} \right]_{(0,0)} k_y h_* \right) + \cos(k_{z_*}^{(0,0)} h_*) \sin \left(\left[\frac{\partial k_{z_*}}{\partial k_y} \right]_{(0,0)} k_y h_* \right) \\ &\approx \sin(k_{z_*}^{(0,0)} h_*) \left\{ 1 - \frac{1}{2} \left[\frac{\partial k_{z_*}}{\partial k_y} \right]_{(0,0)}^2 k_y^2 h_*^2 \right\} + \cos(k_{z_*}^{(0,0)} h_*) \left[\frac{\partial k_{z_*}}{\partial k_y} \right]_{(0,0)} k_y h_* . \end{aligned}$$

From the previous equation, we get

$$\begin{aligned}\sin^2(k_{z_*} h_*)_{\max} &\approx \left[\frac{\partial k_{z_*}}{\partial k_y} \right]_{(0,0)}^2 k_y^2 h_*^2, \\ \sin^2(k_{z_*} h_*)_{\min} &\approx \left\{ 1 - \frac{1}{2} \left[\frac{\partial k_{z_*}}{\partial k_y} \right]_{(0,0)}^2 k_y^2 h_*^2 \right\}^2 \approx \left\{ 1 - \left[\frac{\partial k_{z_*}}{\partial k_y} \right]_{(0,0)}^2 k_y^2 h_*^2 \right\}.\end{aligned}\quad (37)$$

Observing that $\langle k_y^2 \rangle = 1/2 w_0^2$,

$$\begin{aligned}\delta[h_* \lesssim w_0] &= |T_{up} T_{down}|_{(0,0)}^2 \left\{ \frac{1}{1 + \left[\frac{q_{z_*}^2 - k_{z_*}^2}{2 q_{z_*} k_{z_*}} \right]_{(0,0)}^2 \left[\frac{\partial k_{z_*}}{\partial k_y} \right]_{(0,0)}^2 \frac{h_*^2}{2 w_0^2}} - \right. \\ &\quad \left. \frac{1}{1 + \left[\frac{q_{z_*}^2 - k_{z_*}^2}{2 q_{z_*} k_{z_*}} \right]_{(0,0)}^2 \left(1 - \left[\frac{\partial k_{z_*}}{\partial k_y} \right]_{(0,0)}^2 \frac{h_*^2}{2 w_0^2} \right)} \right\}.\end{aligned}\quad (38)$$

Finally,

$$\frac{\delta[h_* \lesssim w_0]}{\Delta[h_* \ll w_0]} = 1 - \left\{ 2 + \left[\frac{(q_{z_*}^2 - k_{z_*}^2)^2}{2 q_{z_*} k_{z_*} (q_{z_*}^2 + k_{z_*}^2)} \right]_{(0,0)}^2 \right\} \left[\frac{\partial k_{z_*}}{\partial k_y} \right]_{(0,0)}^2 \frac{h_*^2}{2 w_0^2}.\quad (39)$$

This new formula shows as the plane wave resonance interval changes when h_* approaches the beam waist w_0 , i.e. in the limit of *partial coherence*.

VIII. CONCLUSIONS

In this paper, we have developed the mathematical formalism which allows to describe the propagation of gaussian lasers beam through a dielectric structure composed by two right angle prisms. Under certain conditions, $h_* \ll w_0$, the plane wave formulas, Eqs.(24), represent a good approximation and the resonance phenomenon can be seen. In this case the peaks of the incident and transmitted beams are clearly related. In the incoherence limit, when multiple diffusion appears, the relative power of the outgoing beam is not more dependent on the air gap interspace, see Eqs. (24). In this case, only the first transmitted beam peak is related to the incoming beam. The secondary transmitted beams are related to the loop factor reflection given by the multiple diffusion of the beam which propagates in the dielectric air gap. The numerical analysis confirms our analytical predictions for the wave and particle limit and shows the damped oscillation transition between these limits.

We hope that the material presented in our study be useful to stimulate and prepare experimental setups to perform qualitative and quantitative measurements to be used to confirm the results presented in our theoretical discussion of gaussian *He-Ne* laser propagation through two dielectric (BK7 or Fused Silica) prisms. Due to the analogy between optics and quantum mechanics [10], the partial coherence limit could also play an important role in the study of transit time in periodic structure and consequently to shed new light on the discussion on superluminal transmission [28–30].

ACKNOWLEDGEMENTS

The authors thank the CNPq, grant PQ2/2013 (S.D.L), and FAPESP, grant 2011/08409-0 (S.A.C) for financial support. The author also thanks the referees for their suggestions and one of the referee for drawing attention to the case of *partial* coherence which is discussed at the end of section VII.

REFERENCES

- [1] E. Pfléghaar, A. Marseille, and A. Weis, *Quantitative investigation of the effect of resonant absorbers on the Goos-Hanchen shift*, Phys. Rev. Lett. **70**, 2281-2284 (1993).
- [2] O. Emile, T. Galstyan, A. Le Floch, and F. Bretenaker *Measurement of the nonlinear Goos-Hanchen effect for Gaussian optical beams*, Phys. Rev. Lett. **75**, 1151-1153 (1995).
- [3] T. Sakata, H. Togo, and F. Shimokawa, *Reflection-type 2×2 optical waveguide switch using the Goos-Hanchen shift effect*, Appl. Phys. Lett. **76**, 2841-2843 (2000).
- [4] C. F. Li, *Negative lateral shift of a light beam transmitted through a dielectric slab and interaction of boundary effects*, Phys. Rev Lett. **91**, 133903-4 (2003).
- [5] C. F. Li and Q. Wang, *Prediction of simultaneously large and opposite generalized Goos-Hanchen shifts for TE and TM light beams in an asymmetric prism configuration*, Phys. Rev. E **69**, 055601-4 (2004) .
- [6] X. Liu, X. Sun, and P. Gu, *Enhanced superprism effect based on positive/negative lateral shift of reflective beam in a FabryPerot filter*, opt. Lett. **32**, 2312-2323 (2007).
- [7] X. Chen, *Electronic analogy of the Goos-Hanchen effect: a review*, J. Opt. **15**, 0333001-13 (2013).
- [8] K. W. Chiu and J. J. Quinn, *On the Goos-Hanchen Effect: A Simple Example of a Time Delay Scattering Process*, Am. J. Phys. **40**, 1847-1851 (1972).
- [9] D. Dragoman, *Phase space correpondence between classical optics and quantum mechanics*, Prog. Opt. **42**, 424-486 (2002).
- [10] S. Longhi, *Quantum-optical analogies using photonic structures*, Las. Phot. Rev. **3**, 243261 (2009),
- [11] S. De Leo and P. Rotelli, *Localized beams and dielectric barriers*, J. Opt. A **10**, 115001-5 (2008).
- [12] S. De Leo and P. Rotelli, *Laser interaction with a dielectric block*, Eur. Phys. J. D **61**, 481-488 (2011).
- [13] S. Zhu, A. W. Yu, D. Hawley, and R. Roy, *Frustrated total internal reflection: A demonstration and review*, Am. J. Phys. **54**, 601-607 (1986)
- [14] P. Balcou, L. Dutriaux, F. Bretenaker, and A. Le Floch, *Frustrated total internal reflection of laser eigenstates*, JOSA B **13**, 1559-1568 (1996).
- [15] A. Haibel, G. Nimtz and A. A. Stahlhofen, *Frustrated total reflection: The double-prism revisited*, Phys. Rev. E **63**, 047601-3 (2001).
- [16] F. P. Zanella, D. V. Magalhaes, M. M. Oliveira, R. F. Bianchi, L. Misoguti, and C. R. Mendonca, *Frustrated total internal reflection: A simple application and demonstration*, Am. J. Phys. **71**, 494-496 (2003).
- [17] D. A. Papathanassoglou and B. Vohnsen, *Direct visualization of evanescent optical waves*, Am. J. Phys. **71**, 670-677 (2003).
- [18] Z. Vörös and R. Johnsen, *A simple demonstration of frustrated total internal reflection*, Am. J. Phys. **76**, 746-749 (2008).

- [19] Y. You, X. Wang, S. Wang, Y. Pan, and J. Zhou, *A new method to demonstrate frustrated total internal reflection in the visible band*, Am. J. Phys. **76**, 224-228 (2008).
- [20] M. Born and E. Wolf, *Principles of optics*, Cambridge UP, Cambridge (1999).
- [21] B. E. A. Saleh and M. C. Teich, *Fundamentals of photonics*, John Wiley & Sons, New York (2007).
- [22] G. B. Arfken and H. J. Weber, *Mathematical Methods for Physicists*, Academic Press, San Diego (2005).
- [23] C. C. Tannoudji, B. Diu and F. Lalöe, *Quantum Mechanics*, Wiley, Paris (1977).
- [24] D. J. Griffiths, *Introduction to quantum mechanics*, Prentice Hall, New York (1995).
- [25] S. De Leo and P. Rotelli, *Resonant laser tunneling*, Eur. Phys. J. D **65**, 563-570 (2011).
- [26] A. Bernardini, S. De Leo, and P. Rotelli, *Above barrier potential diffusion*, Mod. Phys. Lett. A **19**, 2717-2725 (2004).
- [27] S. De Leo and P. Rotelli, *Above barrier Dirac multiple scattering and resonances*, Eur. Phys. J. C **46**, 551-558 (2006).
- [28] J. Ruiz, M. Ortuno, E. Cuevas, and V. Gasparian, *Traversal time as a function of the size of the wavepacket*, J. Phys. I France **7**, 653-661 (1997).
- [29] X. Chen and C.F. Li, *The reflection and transmission group delay times in an asymmetric single quantum barrier*, Eur. Phys. J. B **46**, 433440 (2005).
- [30] X. Chen and C.F. Li, *Superluminal traversal time and interference between multiple finite wave packets*, Eur. Phys. Lett. **82** 30009-6 (2008).

Table 1							
$\lambda = 632.8 \text{ nm}$							
BK7 [$n = 1.515$]				Fused Silica [$n = 1.457$]			
$h_* [\mu\text{m}]$	$\sin \theta_1$	$\sin \theta_2$	$\sin \theta_3$	$h_* [\mu\text{m}]$	$\sin \theta_1$	$\sin \theta_2$	$\sin \theta_3$
1	-0.16457	-0.37333	-0.82546	1	-0.11121	-0.32521	-0.78345
2	-0.11436	-0.16457	-0.24960	2	-0.05940	-0.11121	-0.19862
5	-0.10038	-0.10837	-0.12170	5	-0.04495	-0.05321	-0.06698
10	-0.09839	-0.10038	-0.10371	10	-0.04288	-0.04495	-0.04839

Table 1: Wave-like behavior and coherent interference. First resonance angles for the down-side outgoing *He-Ne* beam interacting with the dielectric structure composed by two BK7 and Fused Silica right angle prisms.

Table 2			
$\theta [\frac{\pi}{12}]$	P_{down}/P_0 - BK7	$\theta [\frac{\pi}{12}]$	P_{down}/P_0 - Fused Silica
-1	0.62150	-1	0.70757
-2	0.74707	-2	0.79369
-3	0.73158	-3	0.77231
-4	0.61046	-4	0.65309
-5	0.32396	-5	0.35841

Table 2: Particle-like behavior and multiple diffusion. Relative down-side outgoing beam power for the *He-Ne* beam interacting with the dielectric structure composed by two BK7 and Fused Silica right angle prisms.

Table 3									
$\lambda = 632.8 \text{ nm}$									
•		P_{down}/P_0 - BK7				•		P_{down}/P_0 - Fused Silica	
$h_* [\mu\text{m}]$	$\theta = \theta_c$	$\theta = -\frac{\pi}{36}$	$\theta = -\frac{\pi}{60}$	$\theta = 0$	$h_* [\mu\text{m}]$	$\theta = \theta_c$	$\theta = -\frac{\pi}{90}$	$\theta = 0$	$\theta = \frac{\pi}{60}$
1	2.78 [2]	1.69 [2]	4.09 [3]	7.19 [4]	1	3.25 [2]	2.32 [2]	5.66 [3]	1.01 [3]
2	7.12 [3]	1.20 [3]	2.25 [5]	3.48 [7]	2	8.34 [3]	2.41 [3]	4.09 [5]	6.39 [7]
5	1.15 [3]	6.46 [7]	3.80 [12]	3.95 [17]	5	1.34 [3]	5.03 [6]	1.58 [11]	1.61 [16]
10	2.87 [4]	2.34 [12]	1.97 [23]	1.05 [33]	10	3.37 [4]	1.81 [10]	3.22 [22]	1.61 [32]

Table 3: Tunneling of light. Relative down-side outgoing beam power for the *He-Ne* beam interacting with the dielectric structure composed by two BK7 and Fused Silica right angle prisms. In the table $[num]$ stands for 10^{-num} . By decreasing the air gap distance between the right angle prisms and/or the incidence angle, we experience the phenomenon of frustrated total internal reflection.

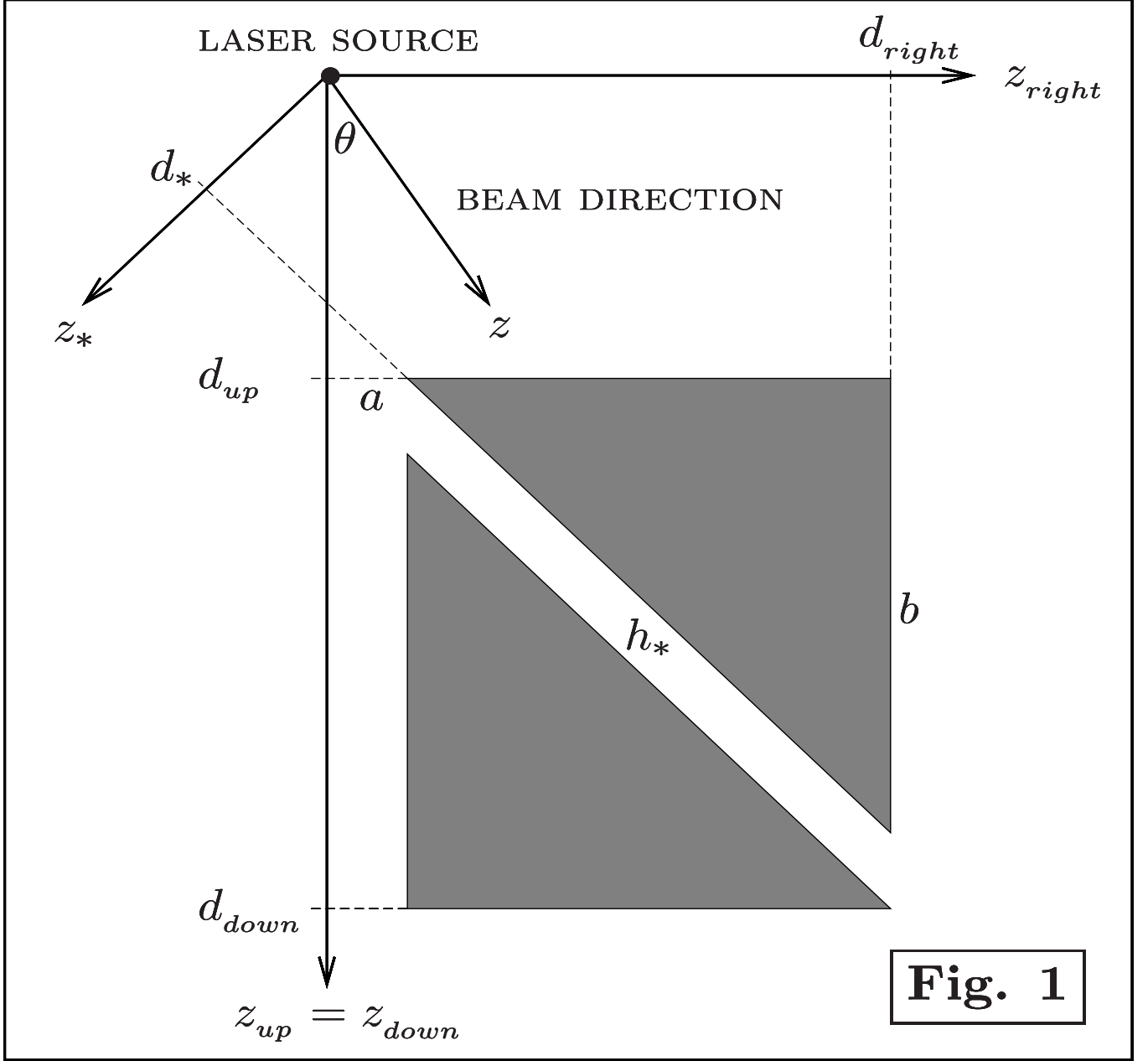


Figure 1: Geometric layout of the dielectric structure analyzed in this paper. The two right angle prisms are separated by a narrow air gap. Depending on the incidence angle, θ , and on the air gap dimension, h_* , the power of the down/right-side outgoing beams will exhibit resonance, multiple diffusion and tunneling phenomena.

Relative power contour plots for the down/right-side outgoing *He-Ne* beams

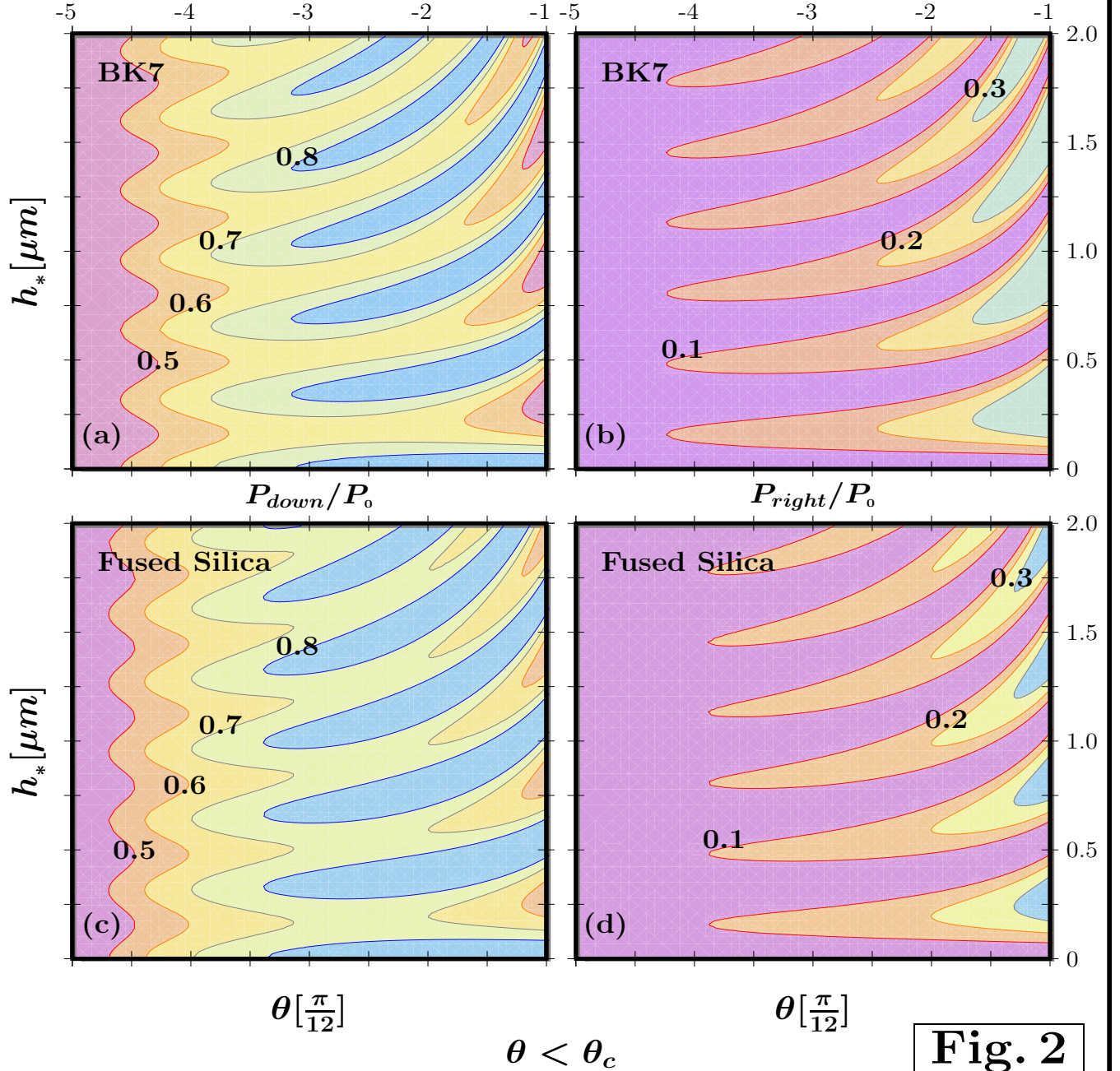


Fig. 2

Figure 2: Relative power contour plots for the plane wave limit ($h_* \ll w_0$) for which wave-like properties can be seen. For $\theta < \theta_c$, the waves which propagate across the air gap are oscillatory and consequently the phenomenon of resonance appears. The contour plots show that for a fixed interval of incidence angles the numbers of the resonances increase by increasing the air gap space between the two right angle prisms and that for given air gap the resonance width increases for decreasing incidence angle.

Relative power contour plots for the down/right-side outgoing *He-Ne* beams

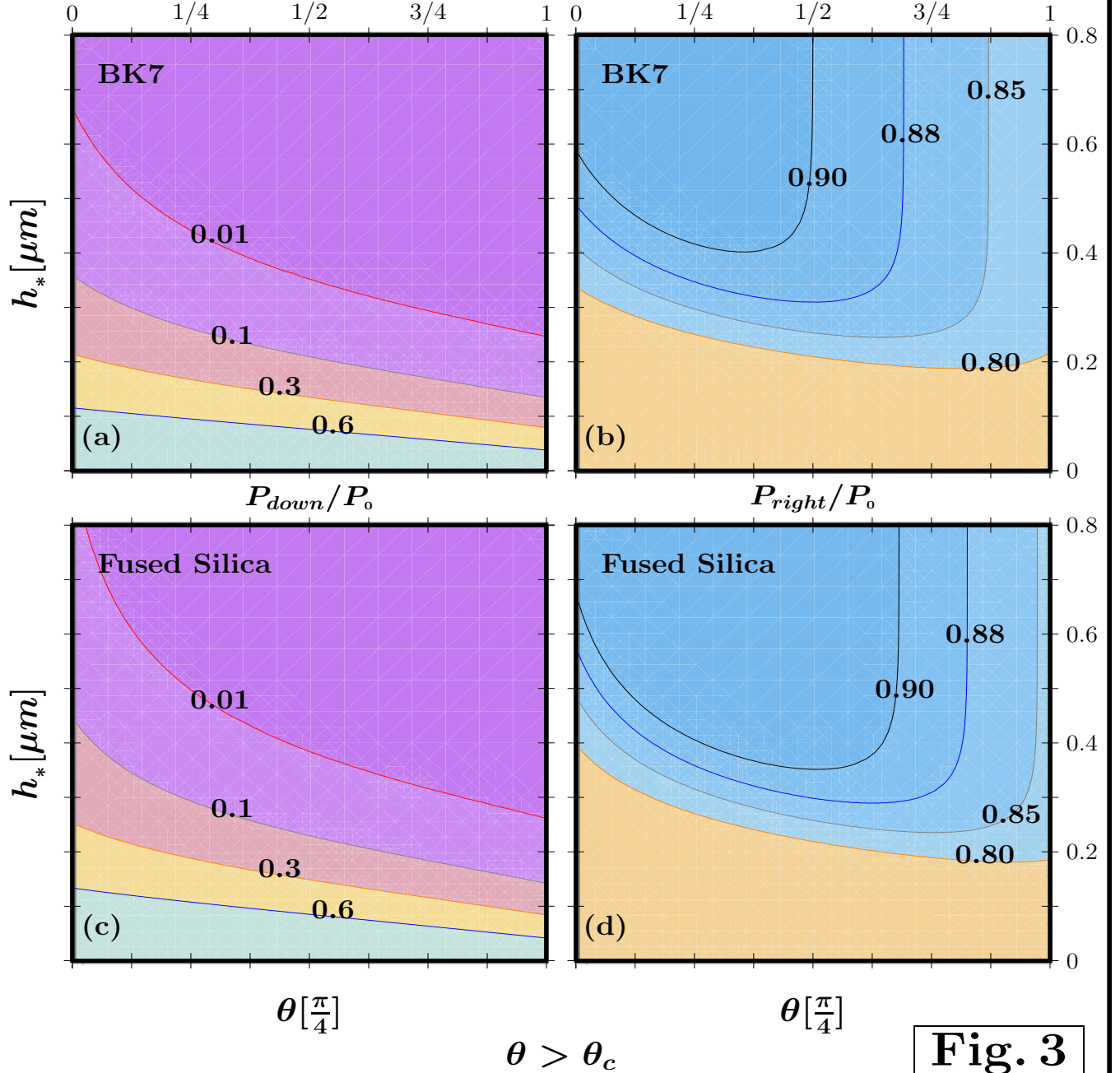


Figure 3: Relative power contour plots for tunneling. For $\theta > \theta_c$, the waves which propagate across the air gap are evanescent and consequently the phenomenon of frustrated total internal reflection appears for the down-side outgoing beam. The contour plots show that this effect is amplified for decreasing values of the air gap distance between the right angle prisms and/or of the incidence angle. From the contour plots is also clear that experiments with incidence angles near to critical angles are more favorable to show the phenomenon of frustrated total internal reflection.

Wave and particle-like behavior for the down-side outgoing *He-Ne* beam

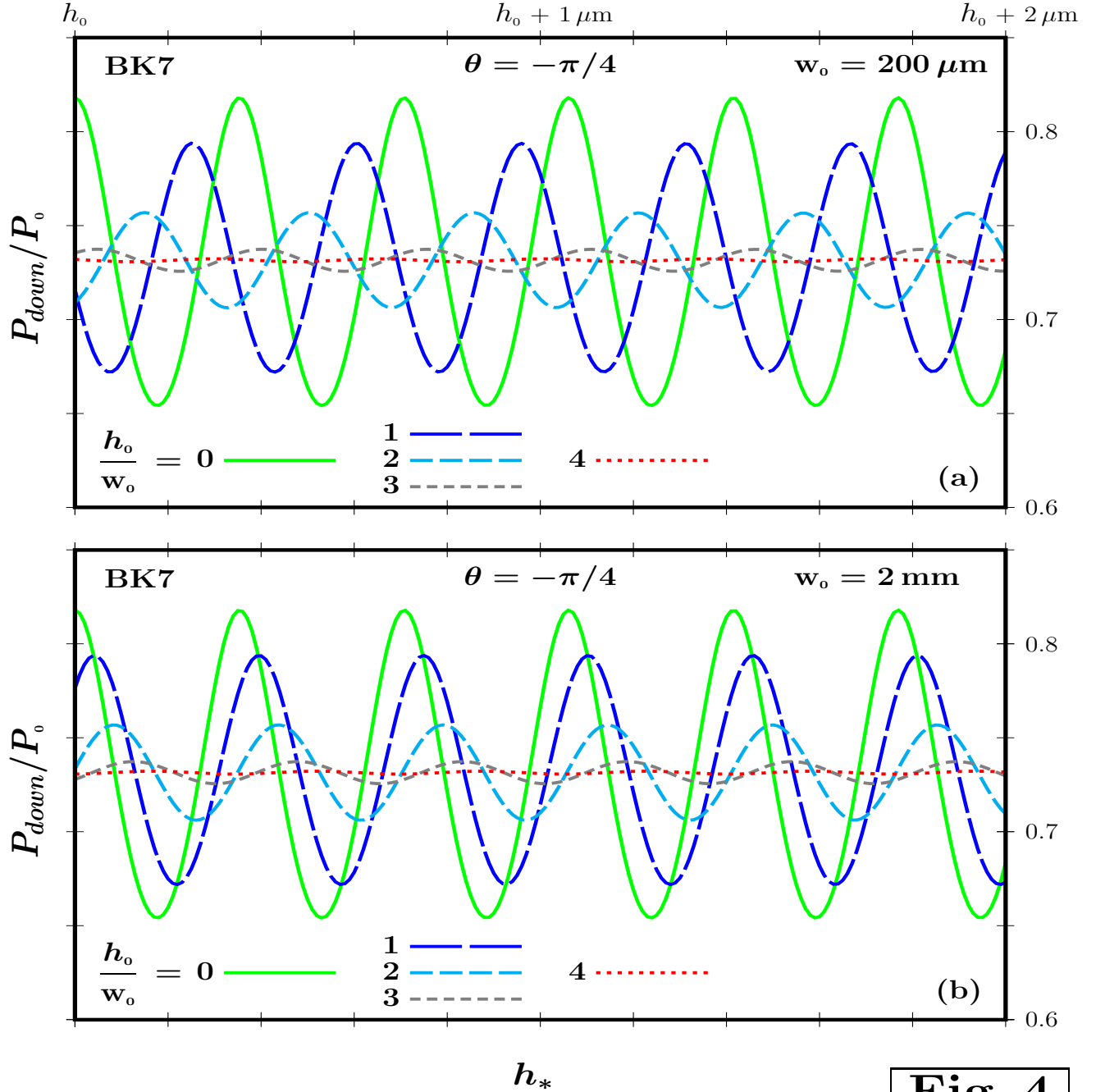


Fig. 4

Figure 4: The relative power for the down-side outgoing beam propagating through BK7 right angle prisms is plotted for different values of the air gap which separates the dielectric blocks. For small values of h_* ($h_0 = 0$), we find the typical resonance curves of the plane wave analysis. For increasing values of h_* ($h_0/w_0 = 1, 2, 3$), the amplitude of the oscillations decreases approaching, for $h_0 = 4 w_0$, the particle limit of Table 2 (≈ 0.732). The numerical analysis confirms our theoretical predictions.

Wave and particle-like behavior for the down-side outgoing *He-Ne* beam

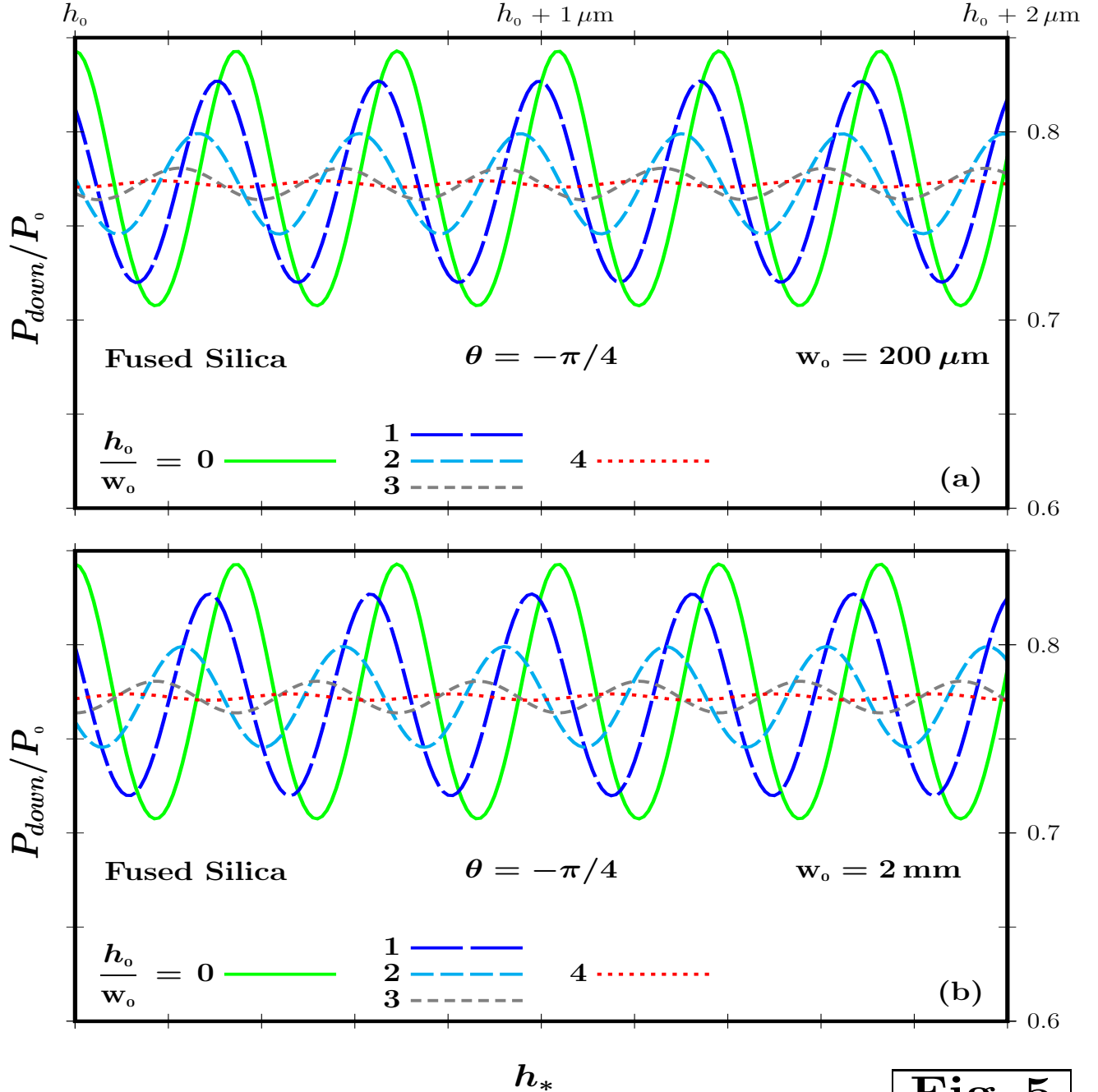


Fig. 5

Figure 5: The relative power for the down-side outgoing beam propagating through Fused Silica right angle prisms is plotted for different values of the air gap which separates the dielectric blocks. For small values of h_* ($h_0 = 0$), we find the typical resonance curves of the plane wave analysis. For increasing values of h_* ($h_0/w_0 = 1, 2, 3$), the amplitude of the oscillations decreases approaching, for $h_0 = 4w_0$, the particle limit of Table 2 (≈ 0.772). The numerical analysis confirms our theoretical predictions.